

Coincidence of reciprocal lattice planes model for quasicrystal-crystal epitaxy

E. J. Widjaja* and L. D. Marks

Department of Materials Science and Engineering, Northwestern University, Cook Hall, 2220 Campus Drive, Evanston, Illinois 60208-3108, USA

(Received 12 March 2003; revised manuscript received 10 June 2003; published 24 October 2003)

A coincidence of reciprocal lattice planes model was developed to calculate the interfacial energy in quasicrystal-crystal epitaxy. This model allows a quantitative description of the interface as opposed to previously employed qualitative models that consider symmetry relations and alignment of rotation axes. Computations were carried out on several types of quasicrystal-crystal systems, namely, the crystalline structures on various surfaces of single quasicrystals (Al-Cu-Fe, Al-Ni-Co, and Al-Cu-Co) caused by ion bombardment, the crystalline thin films grown on quasicrystal substrates, and the quasicrystalline thin films grown on crystalline substrates. This model can also be extended to include quasicrystal-quasicrystal epitaxy.

DOI: 10.1103/PhysRevB.68.134211

PACS number(s): 61.44.Br, 05.70.Np, 68.35.-p

I. INTRODUCTION

Shortly after the discovery of quasicrystals, it was established that the structure of icosahedral Al-Mn undergoes a phase transition when exposed to irradiation of energetic particles.¹ Bombardment with Ar⁺ ions at room temperature transforms the quasicrystalline surface into a crystalline cubic structure due to preferential sputtering of the Al atoms from the surface. The resultant crystalline structure has a specific orientation relationship with respect to the quasicrystalline substrate. Similar behavior has been observed in other quasicrystal systems such as decagonal Al₇₀Ni₁₅Co₁₅,^{2,3} icosahedral Al₆₅Cu₂₀Fe₁₅,^{4,5} decagonal Al₇₀Cu₁₅Co₁₅,^{6,7} and decagonal Al₇₅Ni₁₀Fe₁₅.⁸ Many studies have been devoted to determining the orientational relationship between the quasicrystal and crystal phases by means of transmission electron microscopy,^{3,4,6,7} low-energy electron diffraction,⁵ secondary electron imaging,² and reflection high-energy electron diffraction.⁹⁻¹¹ Recently it was shown that crystalline thin-film growth on quasicrystalline substrates, and vice versa, exhibits the same phenomena.^{9,12}

A majority of these works, however, explain the observed orientation of the structures from a stereographic projection through a description of the rotation axis alignment. While this is a valid approach for describing the orientation, this method offers no insight into the fundamental mechanism behind the preferred orientation. Shimoda *et al.*,⁹ Zurkirch *et al.*,² and Bolliger *et al.*¹³ described their findings via an atomic model of the two-dimensional interface between the quasicrystal and crystal phases, which is obtained by superimposing the surface structures. The validity of these atomic models relies heavily on a real-space structural model for the quasicrystal system, which may not be readily available or, in some cases, may not be correct. Furthermore, their models fall short of the long-range fitting for the superimposed structure since the misfit dislocations and interface relaxations are ignored. Shen *et al.*⁵ explained the orientation relationship between different surfaces of icosahedral Al-Cu-Fe system and its cubic phase via a structural model of cubic close packed and icosahedral packed clusters. This approach allows only one orientation for any given system; this is in contrast to observations where multiple orientations were ob-

served, even for the same surfaces, for example, the Al-Ni-Co 2D surface.³ It should be noted that all of the methods employed to date do not take into account the role of the interfacial energy. Thus, there is a need to develop an improved model that will enhance the fundamental understanding of quasicrystal-crystal epitaxy. In this paper we describe and employ the coincidence reciprocal lattice planes (CRLP) model to predict and explain the orientation relationship in quasicrystal-crystal epitaxy through the inclusion of the interfacial energy.

II. COINCIDENCE RECIPROCAL LATTICE PLANE MODEL FOR QUASICRYSTALS

A very simplistic view of the epitaxial growth places importance upon the principle that the coherent overgrowth of crystal material *Y* on crystal *X* is likely to occur if some undistorted crystal plane of *Y* can be laid down on top of the exposed face of *X*, in such a way that a large fraction of the *Y* atoms can be made to coincide with the sites of *X* atoms. It can be further understood that the greater the number of coincidences per unit area, the lower the energy of the resulting interface will be. This basic principle is the backbone of the coincidence-site-lattice (CSL) theory which was first investigated by Friedel,¹⁴ and later explored by Ranganathan¹⁵ and applied to cubic lattices by Grimmer.¹⁶⁻¹⁹ The CSL concept was implicitly incorporated in the approach of superimposing real-space atomic models employed by Shimoda *et al.*, Zurkirch *et al.* and Bolliger *et al.* Nonetheless their approach lacks the theoretical mathematical expressions that include interfacial energy. In earlier work by Warrington *et al.*,²⁰ a CSL theory was applied to investigate grain boundaries in icosahedral quasicrystals. The CSL method employed is an *N*-dimensional CSL (Ref. 21) due to the quasiperiodic nature of quasicrystals. The focus of this work is to determine the quasicrystal rotations in order to classify disorientation and to find the degeneracy of different values of the coincidence index. However, such *N*-dimensional approach does not offer the potential to solve the problems associated with interfacial energy in the systems; hence a three-dimensional (3D) structural description needs to supplement the hypercrystal description.²²

Given that the nature of the system is quasiperiodic, the 3D reciprocal space of quasicrystals can be mathematically described through a projection from a periodic higher dimension. In addition to that, the reciprocal space also can be directly deduced from electron-diffraction patterns. The 3D approach in a CRLP model for a quasicrystal-crystal interface enables the calculation of the interfacial energy in a similar approach to a crystal-crystal epitaxy. We employ this reciprocal space approach to explain the experimentally observed orientation preference. The improved CRLP model is based on the crystal-crystal epitaxy model previously developed by Fletcher,²³ which will be shown also to be applicable to quasicrystal-crystal epitaxy. The original CRLP model by Fletcher and Lodge²⁴ was exploited as the starting point, as described in the following paragraphs.

The potential energy V_o of a Y atom at position \mathbf{r} outside a plane face of a X crystal with atomic positions \mathbf{R} , $V_o(\mathbf{r})$ can be written in terms of its Fourier components $V_o(\mathbf{k})$ as

$$V_o(\mathbf{r}) = \frac{N}{8\pi^3} \int V_o(\mathbf{k}) \exp(i\mathbf{k} \cdot \mathbf{r}) d\mathbf{k}, \quad (1)$$

$$V_o(\mathbf{k}) = \frac{1}{N} \sum_{\mathbf{R}}^- v(\mathbf{k}) \exp(-i\mathbf{k} \cdot \mathbf{R}), \quad (2)$$

where N is the (infinite) number of atoms in the crystal and $v(\mathbf{k})$, the Fourier transform of the atomic potential $v(\mathbf{r})$, is given by

$$v(\mathbf{k}) = \int v(\mathbf{r}) \exp(-i\mathbf{k} \cdot \mathbf{r}) d\mathbf{r}. \quad (3)$$

Assuming the crystals to be undistorted, the total interaction energy between two crystals, E_o^T , can be expressed through the summation of $V_o(\mathbf{r})$ over all the atomic position \mathbf{R}' of the Y crystal, resulting in

$$\begin{aligned} E_o^T &= \sum_{\mathbf{R}'}^+ V_o(\mathbf{R}') \\ &= \frac{1}{8\pi^3} \sum_{\mathbf{R}'}^+ \sum_{\mathbf{R}}^- \int v(\mathbf{k}) \exp[i\mathbf{k} \cdot (\mathbf{R}' - \mathbf{R})] d\mathbf{k}, \end{aligned} \quad (4)$$

where the plus and minus signs on the summations indicate that it extends only over the upper and the lower half space, respectively.

The equation to describe the interfacial energy per unit area, E_o , can then be simplified to

$$\begin{aligned} E_o &= \frac{1}{2\pi AA'} \delta_{\mathbf{k}_s, \mathbf{q}_s} \delta_{\mathbf{k}_s, \mathbf{q}'_s} \exp(i\mathbf{k}_s \cdot \mathbf{B}_s) \sum_{\mathbf{R}'_3}^+ \sum_{\mathbf{R}_3}^- \int v(\mathbf{k}) \\ &\quad \times \exp[ik_3(R'_3 - R_3 + B_3)] dk_3, \end{aligned} \quad (5)$$

with a sum over all surface reciprocal lattice vectors for each crystal \mathbf{q}_s and \mathbf{q}'_s , where A and A' are areas of the surface unit cells, \mathbf{B} is the relative translation of the two lattices, the subscript 3 represents the component of a vector normal to the interface, \mathbf{R} and \mathbf{R}' have been redefined such that each is

measured from an origin fixed on a lattice point of its respective crystal, \mathbf{R}_s and \mathbf{R}'_s are the associated surface lattice vectors, and \mathbf{k}_s is the component of \mathbf{k} parallel to the surface.

We will now allow elastic displacement of atoms near the interface with a displacement of

$$F(\mathbf{R}) = - \sum_{\kappa}^+ 2[D_{\kappa} \sin(\boldsymbol{\kappa} \cdot \mathbf{R}) + C_{\kappa} \cos(\boldsymbol{\kappa} \cdot \mathbf{R})] - C_o, \quad (6)$$

where κ is a vector corresponding to allowed distortion components. Thus, the interfacial energy described in Eq. (4) becomes

$$E_o^T = \frac{1}{8\pi^3} \sum_{\mathbf{R}'}^+ \sum_{\mathbf{R}}^- \int v(\mathbf{k}) \exp[i\mathbf{k} \cdot (\mathbf{R}' + \mathbf{F}' - \mathbf{R} - \mathbf{F})] d\mathbf{k}. \quad (7)$$

Repeating the same procedure applied to Eq. (4) to result in Eq. (5), Eq. (7) can be transformed for a simple basis into

$$\begin{aligned} E_o &= \frac{1}{2\pi AA'} \sum_{\mathbf{k}_s} V_o(\mathbf{k}_s, B_3) \exp(i\mathbf{k}_s \cdot \mathbf{B}_s) \\ &\quad \times \left\{ \prod_{\kappa} J_0(2\mathbf{k} \cdot \mathbf{D}_{\kappa}) J_0(2\mathbf{k} \cdot \mathbf{C}_{\kappa}) \right\} \\ &\quad \times \left\{ \prod_{\kappa} J_0(2\mathbf{k} \cdot \mathbf{D}'_{\kappa}) J_0(2\mathbf{k} \cdot \mathbf{C}'_{\kappa}) \right\} \\ &\quad \times \left\{ \delta_{k_s, q_s} \delta_{k_s, q'_s} + \sum_{n=1}^{\infty} \sum_{\kappa}^+ \left[\frac{J_n(2\mathbf{k}_s \cdot \mathbf{D}_{\kappa})}{J_0(2\mathbf{k}_s \cdot \mathbf{D}_{\kappa})} \right. \right. \\ &\quad \left. \left. + i^n \frac{J_n(2\mathbf{k}_s \cdot \mathbf{C}_{\kappa})}{J_0(2\mathbf{k}_s \cdot \mathbf{C}_{\kappa})} \right] \delta_{q_s + n\kappa, q'_s} \delta_{k_s, q'_s} \right. \\ &\quad \left. + \sum_{n=1}^{\infty} \sum_{\kappa}^+ \left[\frac{J_n(2\mathbf{k}_s \cdot \mathbf{D}'_{\kappa})}{J_0(2\mathbf{k}_s \cdot \mathbf{D}'_{\kappa})} + i^n \frac{J_n(2\mathbf{k}_s \cdot \mathbf{C}'_{\kappa})}{J_0(2\mathbf{k}_s \cdot \mathbf{C}'_{\kappa})} \right] \right. \\ &\quad \left. \times \delta_{q_s + n\kappa, q'_s} \delta_{k_s, q_s} + \dots \right\}. \end{aligned} \quad (8)$$

In Fletcher's original derivation, only a simple basis for the unit cell was employed, and the δ functions arose via a sum over all atoms in the interface, i.e.,

$$\sum_{\mathbf{R}} \exp(i\mathbf{k} \cdot \mathbf{R}) = N \delta_{\mathbf{k}, \mathbf{q}} \quad (9)$$

for N atoms. This is not correct in general, and the equation has to be modified by replacing everywhere $\delta_{k_s, q_s} \delta_{k_s, q'_s}$ by $U(\mathbf{q})U(\mathbf{q}') \times \delta_{k_s, q_s} \delta_{k_s, q'_s}$, where

$$U(\mathbf{q}) = \sum_{\mathbf{R}} \exp(i\mathbf{q} \cdot \mathbf{R}) \quad (10)$$

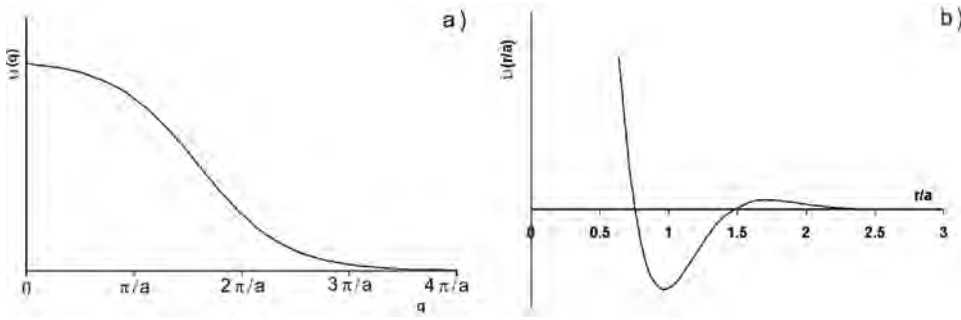


FIG. 1. (a) Fourier transform of the interaction potential model used in this calculation and given in Eq. (12), drawn for $b=a$. (b) The interaction potential in real space.

with a sum over the basis of the unit cell. This term, Eq. (10), which by analogy to crystallographic direct methods, where it also arises, is referred to as a unitary structure factor.²⁵

From Eqs. (8) (after expanding the Bessel functions and keeping first-order terms only) and (10), an energy minimization with respect to \mathbf{D}_k and \mathbf{B} results in an approximate total energy of the form

$$E \approx E_0 - t \sum_{\kappa} \frac{[U(\mathbf{q})v(\mathbf{q})]^2}{\kappa}, \quad (11)$$

where E_0 is the coincidence part of the boundary energy, t is a constant, κ is the vector joining two diffraction spots from the bicrystal, and $v(\mathbf{q})$ is the atomic interaction potential. The constant t , which depends on many parameters such as shear modulus, bulk modulus, and Poisson's ratio, is necessary to calculate an expected value for the total energy; however the value of this constant is not important in our calculations since we consider the relative magnitudes only. Hence, t was chosen arbitrary to give a convenient energy scale. A more complete solution can be obtained by equating the tractions across the interface; we will only use this first-order approximation here.

An accurate interaction potential is unknown at present for the quasicrystal-crystal interface; nevertheless we will use a model potential for exploratory calculations introduced by Fletcher,²⁶ which has the form

$$v(\mathbf{q}) = H \left(\frac{a+b}{a} \right)^3 \{ \exp[2.5q(a+b) - 4] + 1 \}^{-1}, \quad (12)$$

where H is a scale constant and a and b are atomic radii of crystals X and Y , respectively. In this model, only interactions with atoms lying in neighboring planes parallel to the interface are considered; in addition, this potential has a repulsive core which is not so hard. The Fourier transform

$v(\mathbf{q})$ and the direct potential $v(\mathbf{r})$ used are shown in Fig. 1 for the case $a=b$. The model potential in Eq. (12) can be further simplified into

$$v(\mathbf{q}) = \{ \exp[\alpha q - 4] + 1 \}^{-1}, \quad (13)$$

where α is equal to 2.5 ($a+b$); the values of α are tabulated in Table I for all cases in our computations.

III. CALCULATION FOR QUASICRYSTAL-CRYSTAL EPITAXY

The majority of the previous work on quasicrystal-crystal epitaxial systems has been devoted to the epitaxial relationship between crystalline structures on single-grain quasicrystal resulting from ion-bombardment processing. Thermodynamically, the stability of the aforementioned systems is uncertain since the ion-bombardment process is commonly conducted at room temperature. Nevertheless, even with limited thermal energy available to allow atomic movement to achieve a thermodynamically stable interface, the kinetic energy introduced by ion fluxes may supply the required energy. The abundance of literature data on ion-bombarded surfaces is advantageous for analysis, even though these systems do not make ideal case studies.

Recently, studies on the epitaxial relationships between crystalline thin films on quasicrystal substrates via physical vapor deposition have been reported. Shimoda *et al.* attempted to grow Au thin films on decagonal Al-Ni-Co and reported the orientation of the alloyed AuAl₂ layer with respect to the substrates.^{9,10} A similar observation was later reported for PtAl₂.¹¹ Widjaja and Marks presented evidence of epitaxial Al-Cu-Fe-Cr decagonal thin films on atomically flat Al₂O₃ [0001] surface.¹² It appears that these are the only reports on thermodynamically stable epitaxial relationships

TABLE I. Expected value for atomic radii and α . The atomic radii values are based on concentration-weighted atomic radii [calculated using self-consistent-field functions (Refs. 27,28)].

Quasicrystal compound	Atomic radius (Å)	Crystal compound	Atomic radius (Å)	α
Al ₆₅ Cu ₂₀ Fe ₁₅	1.291	Al ₅₀ Cu _x Fe _{1-x}	1.339	6.574
Al ₇₀ Ni ₁₅ Co ₁₅	1.278	Al ₅₀ Ni _x Co _{1-x}	1.343	6.550
Al ₆₅ Cu ₂₀ Co ₁₅	1.226	Al ₅₀ Cu _x Co _{1-x}	1.330	6.390
Al ₇₀ Ni ₁₅ Co ₁₅	1.278	AuAl ₂	1.367	6.610
Al ₇₀ Ni ₁₅ Co ₁₅	1.278	PtAl ₂	1.377	6.635

TABLE II. Orientation relationship in crystal-quasicrystal epitaxy. When there are two alignments given, they are equivalent and correspond to only one unique alignment. "Primary?" indicates if the observed alignment appears as the primary peak (global minimum). "Fit?" indicates whether the calculation matches the experimentally observed configuration.

No.	Quasicrystal		Crystal structure	Parallel axis QC crystal	In-plane alignment				Primary?	Fit?
	System	Structure			Observed	Reference	Calculated			
1	Al-Cu-Fe	Icosahedral	CsCl	$5f [110]$	$2P [1\bar{1}0]-2D [001]$	4	$2P [1\bar{1}0]-2D [001]$	No	Yes	
2	Al-Cu-Fe	Icosahedral	CsCl	$5f [113]$	$2P [1\bar{1}0]$	4	$2P [\bar{1}\bar{2}1]$	Yes	Yes	
3	Al-Cu-Fe	Icosahedral	CsCl	$2f [111]$	$2f [1\bar{2}1]$	33	$5f [1\bar{1}0]$	Yes	Yes	
4	Al-Cu-Fe	Icosahedral	CsCl	$3f [111]$	$3f [1\bar{1}0]$	33	$3f [1\bar{1}0]$	Yes	Yes	
5	Al-Ni-Co	Decagonal	CsCl	$10f [110]$	$2P [001] - 2D [1\bar{1}0]$	3,2	$2P [001]-2D [1\bar{1}0]$	Yes	Yes	
6	Al-Ni-Co	Decagonal	CsCl	$2D [110]$	$10f [1\bar{1}0]-2P [001]$	3	$10f [1\bar{1}0]-2P [001]$	Yes	Yes	
7	Al-Ni-Co	Decagonal	CsCl	$2D [111]$	$10f [1\bar{1}0]$	3	$2P [\bar{2}\bar{1}3]$	Yes	No	
					$10f [1\bar{1}0]$	3	$10f [1\bar{1}0]$	No	Yes	
8	Al-Ni-Co	Decagonal	CsCl	$D [100]$	$2f [001]$	3	$2f [001]$	Yes	Yes	
9	Al-Cu-Co	Decagonal	CsCl	$10f [110]$	$2P [1\bar{1}0]-2D [001]$	7	$2P [1\bar{1}0]-2D [001]$	Yes	Yes	
10	Al-Cu-Co	Decagonal	CsCl	$2P [110]$	$10f [1\bar{1}0]-2D [001]$	7	$10f [1\bar{1}0]-2D [001]$	Yes	Yes	
11	Al-Ni-Co	Decagonal	CsCl	$10f [110]$	$2D [001]-2D [\bar{1}12]$	9,10	$2D [\bar{1}12]$	No	Yes	
			(AuAl ₂)							
12	Al-Ni-Co	Decagonal	CsCl	$10f [110]$	$2D [001]-2D [\bar{1}12]$	11	$2D [\bar{1}12]$	No	Yes	
			(PtAl ₂)							
13	Al-Cu-Fe-Cr	Decagonal	Corundum	$10f [0001]$	$2P [10\bar{1}0]$	12	$2P [10\bar{1}0]$	Yes	Yes	
14	Al-Cu-Fe-Cr	Decagonal	Corundum	$10f [0001]$	$2D [10\bar{1}0]$	12	$2D [10\bar{1}0]$	No	Yes	
			(Al ₂ O ₃)							
			(Al ₂ O ₃)							

in crystal-quasicrystal systems where the interface relationship is well described.²⁹⁻³²

Computations were carried out on various ion-bombarded surfaces for three quasicrystal systems: the icosahedral Al-Cu-Fe system and the decagonal Al-Ni-Co and Al-Cu-Co systems. Calculations were also performed for quasicrystal (QC)-crystal thin-film epitaxy for the following systems: AuAl₂ and PtAl₂ thin films on a tenfold surface of decagonal Al-Ni-Co and decagonal Al-Cu-Fe-Cr thin film on corundum Al₂O₃ [0001]. A complete comparison of the observed and simulated results is tabulated in Table II. Table III summarizes the corresponding calculated results and position of the peaks relative to a set of references.

Quasicrystal reciprocal lattice points and structure factors were simulated using the QUAREF program;³⁴ the 3D reciprocal space quasilattices were generated by a projection method from a higher dimension hypercube. Lattice parameters for the hypercube and the corresponding space group are given in Table IV along with the crystalline structure data.

Calculations of $U(\mathbf{q})$ for quasicrystals were simplified by incorporating only the intrinsic structure factor which is independent of the specific decoration of the lattice due to the complexity of real decorated lattices. Unlike crystalline materials, diffraction patterns of quasicrystals generally cannot be decomposed into the intrinsic structure factor and geometric structure factor.⁴⁰ The former is attributed to the quasilattice, while the latter is due to the decoration.

The values of atomic radii for the crystalline and quasic-

crystalline structures considered in the atomic potential calculation were taken to be the expected values of the systems:

$$\hat{a} = \sum_i x_i a_i, \quad (14)$$

where x_i and a_i are the atomic percentage and radius for element i , respectively, in the compound. Table I contains the calculated values of the expected atomic radii for all systems in this simulation and the corresponding α values.

Another estimate for average values of the atomic radius can be obtained from the density ρ of the alloy:

$$\frac{4}{3} \pi (R_{WS})^3 = \frac{1}{\rho}, \quad (15)$$

where R_{WS} is the average Wigner-Seitz radius. Comparison of the average atomic radius values calculated from concentration-weighted atomic radii [from Eq. (14)], concentration-weighted Wigner-Seitz radii,⁴¹ and density calculations [from Eq. (15)] for the alloys Al_{72.6}Ni_{10.5}Co_{16.9}, Al₇₂Ni₂₀Co₈, and Al₇₀Pd₂₁Mn₉ is tabulated in Table V. Due to the lack of availability of bulk density values for the various alloys used in this study, we used concentration-weighted atomic radii values for all calculations. The difference between these values and the ones from density calculations is about 5% and this has very little effect on the final results.

TABLE III. Peak positions and reference in calculated configurations. “*P*” or “*S*” indicates if the observed peak appears as primary or secondary peak, respectively. “*” denotes the ambiguity of the peak from experimental observation. “-” indicates no special alignment or no significant secondary peak.

No.	Quasicrystal System	Crystal Structure	Crystal structure	Parallel axis QC crystal	Reference 0°	Primary Angle	Alignment	Secondary Angle	Alignment	Observed
1	Al-Cu-Fe	Icosahedral	CsCl	$5f [110]$	$2D [1\bar{1}0]$	$\pm 9.45^\circ$	-	$+18^\circ$	$2P [1\bar{1}0]$	<i>S</i>
2	Al-Cu-Fe	Icosahedral	CsCl	$5f [113]$	$2D [1\bar{1}0]$	$18^\circ \pm 1.2^\circ$	$2P [\bar{1}\bar{2}1]$	0°	$2D [1\bar{1}0]$	<i>P*</i>
3	Al-Cu-Fe	Icosahedral	CsCl	$2f [111]$	$2f [1\bar{2}1]$	$\pm 1.7^\circ$	$5f [1\bar{1}0]$	-	-	<i>P*</i>
4	Al-Cu-Fe	Icosahedral	CsCl	$3f [111]$	$3f [1\bar{1}0]$	0°	$3f [1\bar{1}0]$	-	-	<i>P</i>
5	Al-Ni-Co	Decagonal	CsCl	$10f [110]$	$2P [001]$	0°	$2P [001]$	-	-	<i>P</i>
6	Al-Ni-Co	Decagonal	CsCl	$2D [110]$	$10f [1\bar{1}0]$	0°	$10f [1\bar{1}0]$	-	-	<i>P</i>
7	Al-Ni-Co	Decagonal	CsCl	$2D [111]$	$10f [1\bar{1}0]$	$\pm 19.1^\circ$	$2P [\bar{2}\bar{1}3]$	0°	$10f [1\bar{1}0]$	<i>S</i>
8	Al-Ni-Co	Decagonal	CsCl	$D [100]$	$2f [001]$	0°	$2f [001]$	-	-	<i>P</i>
9	Al-Cu-Co	Decagonal	CsCl	$10f [110]$	$2P [1\bar{1}0]$	0°	$2P [1\bar{1}0]$	-	-	<i>P</i>
10	Al-Cu-Co	Decagonal	CsCl	$2P [110]$	$10f [1\bar{1}0]$	0°	$10f [1\bar{1}0]$	-	-	<i>P</i>
11	Al-Ni-Co	Decagonal	AuAl ₂	$10f [110]$	$2D [001]$	-	-	$\pm 0.7^\circ$	$2D [\bar{1}12]$	<i>S*</i>
12	Al-Ni-Co	Decagonal	PtAl ₂	$10f [110]$	$2D [001]$	-	-	$\pm 0.7^\circ$	$2D [\bar{1}12]$	<i>S*</i>
13	Al-Cu-Fe-Cr	Decagonal	Al ₂ O ₃	$10f [0001]$	$2P [10\bar{1}0]$	0°	$2P [10\bar{1}0]$	$\pm 18^\circ$	$2D [10\bar{1}0]$	<i>P&S</i>

In the calculation, the reciprocal lattice planes for the two crystals were reciprocal surface unit cells. For periodic crystals, reciprocal surface unit cells were constructed under the following simplifications: (1) The surface unit cell was determined based on bulk truncation without any reconstruction. (2) All elements were considered to behave similarly for surfaces containing more than one element. Note that the reciprocal surface unit cells may be denser than those normally observed in bulk electron-diffraction patterns. The reciprocal unit cells included in the calculations are limited to magnitudes less than 1 \AA^{-1} ; \mathbf{q} vectors with larger values are considered negligible due to the exponential decaying nature of the interaction potential as shown in Eq. (13). Since the specific nature of surface interface structures in quasicrystal-line systems is unknown, the surface reciprocal lattices were constructed based on bulk structures; many experiments have confirmed the quasi-periodic nature of the surface.^{45–50}

IV. RESULTS AND DISCUSSIONS

In most cases, calculations showed perfect fits between simulated and observed configurations; exceptions will be

discussed further in this section. Figures 2(a) and 2(b) show a comparison between the calculated and experimentally observed configuration for the ion-sputtered Al-Cu-Fe single-grain quasicrystal fivefold surface. In these plots, surface spots have been eliminated to assist in the visual comparison, however these spots were taken into consideration during the calculations. Experimental observations in other systems can be easily compared to simulated results; references are given in Table II. Numerical data for peak positions, types, and references are given in Table III. Results for the interfacial energy calculation and the corresponding structure for three different cases are plotted in Figs. 3(a)–3(f) as examples. The configurations shown in Fig. 3 match the experimental observation perfectly; surface spots are also removed to ease visual comparison. In all figures, unless otherwise noted: (1) surface spots are removed, (2) the sizes of the spots corresponding to the intensities, however, are not to be scaled, and (3) the gray and black spots represent, respectively, the quasicrystal and crystal spots.

We will look further into the case of ion-sputtered Al-Ni-Co decagonal twofold surface as an example. For this

TABLE IV. Structure and (quasi)lattice data input for calculations.

No.	Quasicrystal		Crystal		Reference	Structure	$a(\text{\AA})$	$c(\text{\AA})$	Reference
	System	Structure	symmetry						
1	Al-Cu-Fe	Icosahedral	$F-3-5$	8.966	35	CsCl	2.942		5
2	Al-Ni-Co	Decagonal	$P10.5/mm$	3.3931	4.807	36	CsCl	2.8	2
							AuAl ₂	5.998	10
							PtAl ₂	5.922	11
3	Al-Cu-Co	Decagonal	$P10.5/mm$	3.368	4.4148	37	CsCl	2.9	6
4	Al-Pd-Mn	Icosahedral	$m-3-5$	9.123	12.06	38			
							Al-Pd-Mn	Decagonal	$P10.5/mmc$
5	Al-Cu-Fe-Cr	Decagonal	Measured experimentally			12	Al ₂ O ₃	4.763 13.003	12

TABLE V. Comparison of calculated average atomic radii (unit in Å) from concentration-weighted atomic radii, concentration-weighted Wigner-Seitz radii, and bulk density measurements. References for the values of density used in radius calculations are given.

Alloys	Eq. (14)	Ref. 41	Eq. (15)
Al _{72.6} Ni _{10.5} Co _{16.9} (Ref. 42)	1.270	1.288	1.337
Al ₇₂ Ni ₂₀ Co ₈ (Ref. 43)	1.269	1.370	1.204
Al ₇₀ Pd ₂₁ Mn ₉ (Ref. 44)	1.326	1.372	1.209

surface, two different out-of-plane alignments have been observed, that is, 2D axis of the decagonal phase parallel to $\langle 110 \rangle$ direction ($2D_{dec} \parallel [110]_{CsCl}$) and parallel to $\langle 111 \rangle$ direction ($2D_{dec} \parallel [111]_{CsCl}$) of the CsCl crystalline phase. Henceforth, the notation $V \parallel [hkl]$ will be used to indicate alignment of the V rotation axis of the quasicrystal phase with $\langle hkl \rangle$ being direction of the crystalline phase and the notations $2D-2P$, $5f$, $10f$, and $3f$ will refer to the two twofold axes rotated relatively to each other by 18° , the fivefold axis, the tenfold axis, and the threefold axis of the quasicrystals, respectively.

In the $2D \parallel [110]$ case, the in-plane alignment of $10f \parallel [1\bar{1}0]-2P \parallel [001]$ is observed and it fits the calculated structure. However, the calculated structure for $2D \parallel [111]$ is $2P \parallel [\bar{2}\bar{1}3]$ while experimental observation is $2P \parallel [\bar{1}\bar{1}2]$ (equivalent to $10f \parallel [1\bar{1}0]$). This observed configuration, which differs from the calculated one, however, appears in the calculation as second minima, with the primary minima positions at $\pm 19.1^\circ$ rotation from them. Figures 4(a) and 4(b) illustrate the calculated structures at both minima; surface reciprocal spots were plotted. Configuration in Fig. 4(b), $10f \parallel [1\bar{1}0]$, which fits the observed data, has a higher number of near plane-coincidence, however Fig. 4(a) with configuration $2P \parallel [\bar{2}\bar{1}3]$ results in much lower energy due to a very small κ value from closer coincidence in one plane. Analysis on the energy graph Fig. 4(c) shows a very sharp peak for the configuration described by Fig. 4(a) [full width at half maximum (FWHM) less than 0.05°] while a wide peak for Fig. 4(b) (FWHM $> 14^\circ$) is evident. This energy

profile allows the system to achieve $10f \parallel [1\bar{1}0]$ alignment relatively easily since only small fluctuation is needed to move the system to this minimum. The simulated configuration in Fig. 4(d) is the case observed in Ref. 3; here, surface spots have been removed and bulk spots are indexed.

Two cases of CsCl structure on icosahedral Al-Cu-Fe, $[113]$ on fivefold and $[111]$ on twofold surfaces were investigated and gave results which differ by less than 2° degrees rotation. This difference may be real, but can also be attributed to mistakes in experimental observation due to small angle differences between the orientations. The angle between $[1\bar{1}0]$ and $[\bar{1}\bar{2}1]$ in CsCl structure is 73.2° and the angle between two $2P$ axes is 72° ; while the angle between $[1\bar{1}0]$ and $[1\bar{2}1]$ in CsCl is 30° and twofold and fivefold axes is 31.7° . In the literature, observations usually reported these configurations, both for $2P \parallel [\bar{1}\bar{2}1]-2P \parallel [1\bar{1}0]$ and $5f \parallel [1\bar{1}0]-2f \parallel [1\bar{2}1]$, to be similar due to their small angle differences. It is ambiguous whether both or only one configuration was observed.

Similarly, for the case in which the $[110]$ CsCl structure on fivefold icosahedral Al-Cu-Fe is observed, the orientation appears as secondary peak (local minimum) instead of the primary minimum in accordance with most of the calculations. Calculations limiting contributing \mathbf{q} 's in reciprocal space up to 0.6 \AA^{-1} resulted in the observed orientation as the lowest energy. For thin-film growth of Au and Al on Al-Ni-Co substrates, calculations showed a similar trend to the case of $[110]$ on the fivefold surface; only by limiting the contributing \mathbf{q} values to 0.6 \AA^{-1} , the simulation matched the experimental data.

This discrepancy can also be attributed to the simplistic nature of the interaction potential form. A more sophisticated and correct model is required to be able to understand the interaction across the interface, and hence be able to predict (and explain) the observed experimental data to a higher accuracy. However, with this simple model we show that we are able to explain the majority of experimentally observed in-plane relationships reported in the literature. In addition to that, there is no justification that the observed orientations should be the global minima of the interfacial energy.

Observations of multiple in-plane alignments for the same

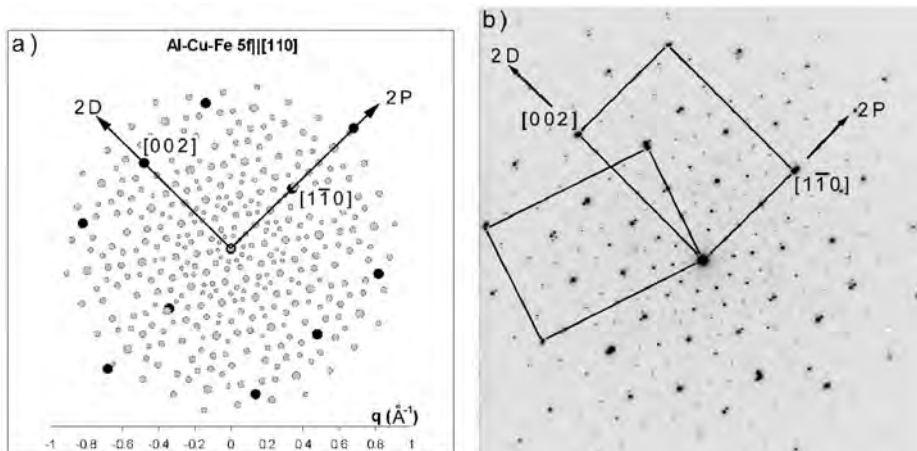


FIG. 2. Comparison between (a) simulated and (b) experimentally observed configurations in ion-sputtered fivefold surface of Al-Cu-Fe quasicrystals. Gray and black spots represent the quasicrystal and crystal spots, respectively.

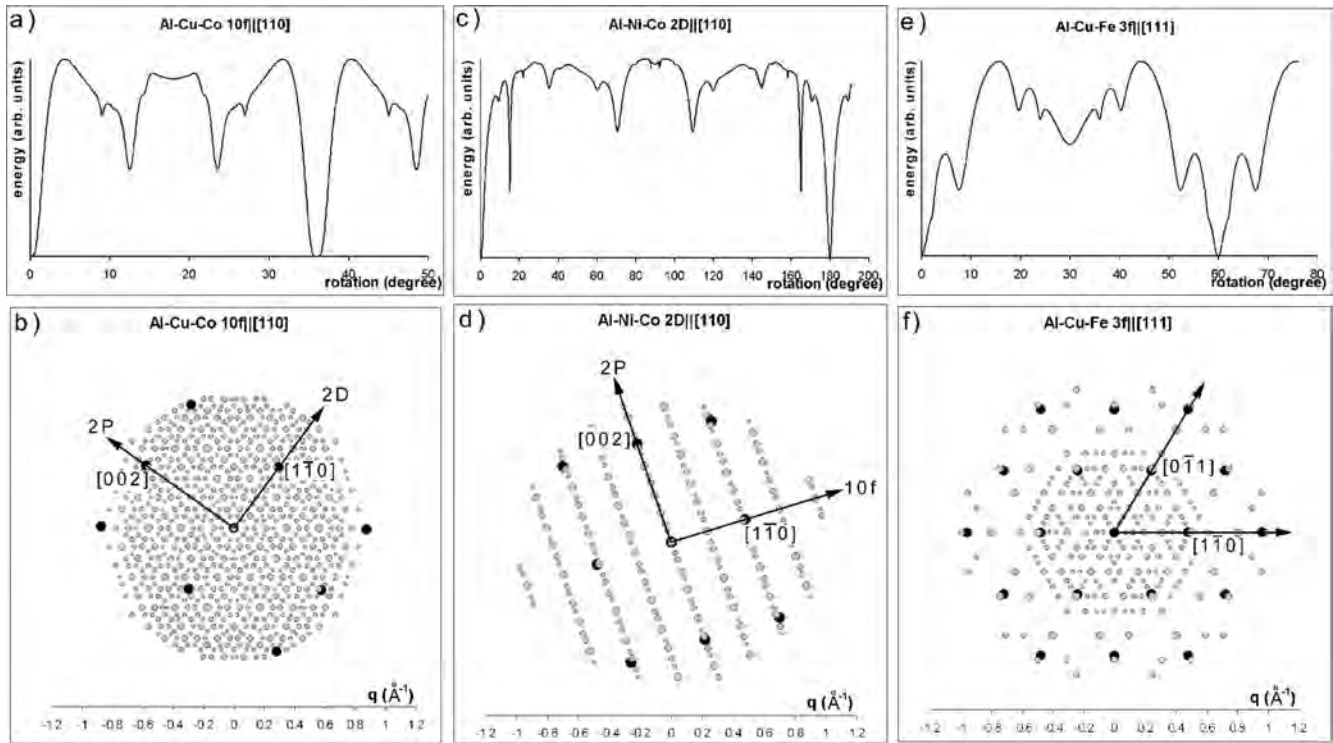


FIG. 3. Interfacial energy calculation and its corresponding structure, respectively, at 0° rotation (which is the minimum) for (a) and (b) Al-Cu-Co $10f\parallel[110]$, (c) and (d) Al-Ni-Co $2D\parallel[110]$, and (e) and (f) Al-Cu-Fe $3f\parallel[111]$; crystal-quasicrystal epitaxy is due to ion bombardments. Gray and black spots represent the quasicrystal and crystal spots, respectively.

out-of-plane alignment have been reported by Widjaja *et al.* for Al-Cu-Fe-Cr decagonal thin films on atomically flat Al_2O_3 substrates.¹² A similar energy calculation showed existence of two unique minima corresponding to two unique in-plane alignments. Each of these configurations has been independently observed experimentally on the same sample.

Using a similar idea for crystal-crystal epitaxy, which we extend to include quasicrystal-crystal epitaxy, we can now move and apply the same approach for quasicrystal-quasicrystal epitaxy. From Eq. (11), the energy actually appears to have an infinite negative value as we approach the coincidence-boundary configuration $\kappa=0$, but the real situation is that the coincidence boundary of any order represents a cusped minimum in the energy. The depth of this minimum depends on the strength of the potential component brought into coincidence. Nevertheless, without the exact knowledge of the potential form and necessity to calculate the value of interface energy, we can predict similar behavior in quasicrystal-quasicrystal epitaxy. The only existing report is Al-Pd-Mn quasicrystals.^{51,52} Menguy *et al.*⁵¹ reported phason-phonon-assisted epitaxy at icosahedral-decagonal interfaces in Al-Pd-Mn quasicrystals. The closeness of their structure has been used as a basis to explain their oriented fivefold/tenfold axis. In this case the lattice planes match very well, as shown in the superimposed simulated 2D reciprocal space patterns for the fivefold and tenfold directions in Fig. 5.

The results reported herein indicate that quasicrystalline materials can have specific orientational relationships in interfaces to crystals, and that these obey very similar rules to

those that govern crystalline interfaces. In real space it is hard to model this (except via some large approximant to the quasicrystal), but the first-order approach is viable and should be completely general in reciprocal space. Equation (11) shows that with appropriate simplification we can find the most probable orientation relationship between a quasicrystal-crystal structure, which is the configuration with a small κ vector, a large interaction potential $\nu(\mathbf{q})$ and a large unitary structure factor $U(\mathbf{q})$. The $U(\mathbf{q})$ term that should be included will weight the analysis towards orientations with more atoms aligned, and may be important in general although often the $1/\kappa$ term will dominate. Only small \mathbf{q} 's are dominant and need to be considered due to exponential decay of interaction potential $\nu(\mathbf{q})$. By simple calculation one can find relatively easily the most stable configuration. However, as shown in some cases in our computations, the most stable configuration is not always the experimentally observed configuration. This can be explained by an analysis of the kinetics.

Due to the difference in \mathbf{q} vectors of quasicrystals and crystals, which is the κ vector, dislocations are created to accommodate the strain. Unlike the observations of dislocations in quasicrystal phases, only a few papers have reported the study of interfacial dislocation in quasicrystal-crystal epitaxy.^{6,8,53} Zhuang *et al.*⁸ reported the observation of misfit dislocations between the B2 surface layer and the decagonal $\text{Al}_{75}\text{Ni}_{10}\text{Fe}_{15}$ which are parallel but less regularly spaced. They observed two types of spacing with a distance ratio of the golden mean of $(1+\sqrt{5})/2$, which were attributed to

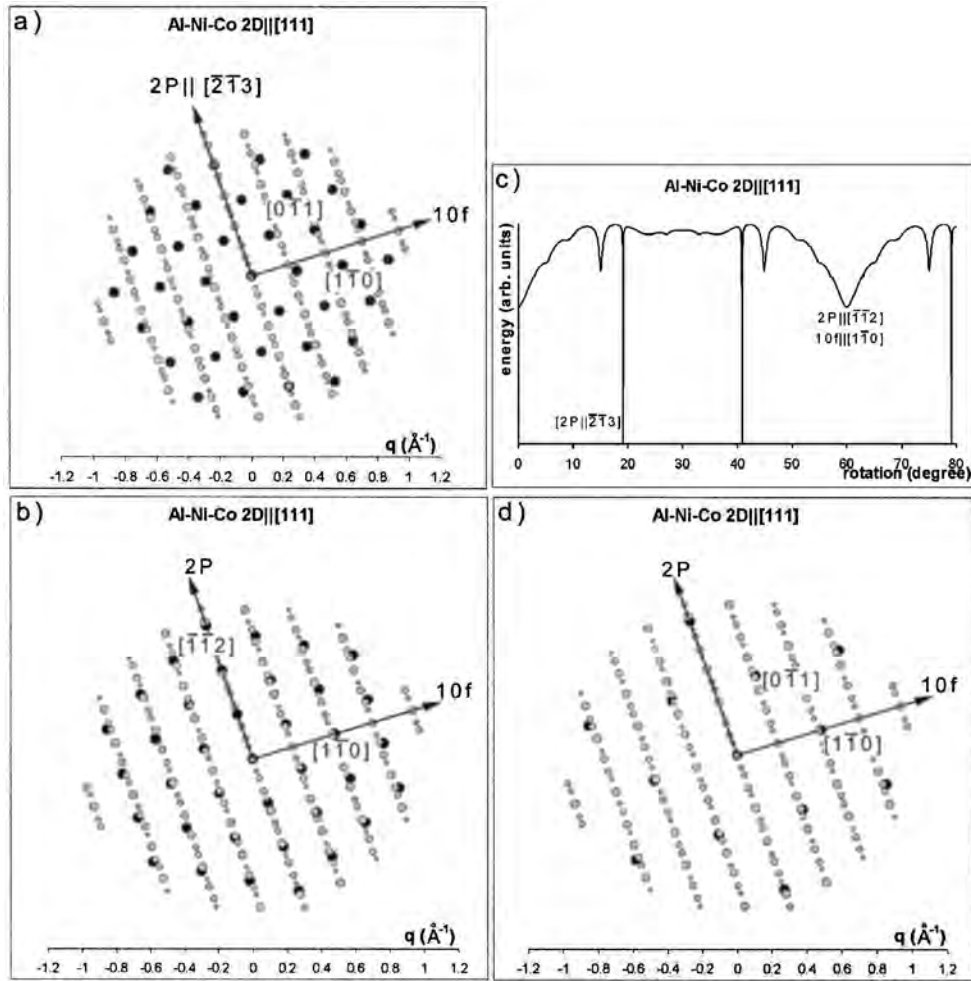


FIG. 4. Comparison of two simulated configurations at two different minima for Al-Ni-Co 2D||[111]. (a) Configuration at the lowest energy at 19.1° and (b) at the other minimum at 0°; interfacial energy calculation is shown in (c) and experimentally observed configuration in (d). Directions for twofold axis for quasicrystals are given and diffraction spots for the crystal are indexed. Gray and black spots represent the quasicrystal and crystal spots, respectively.

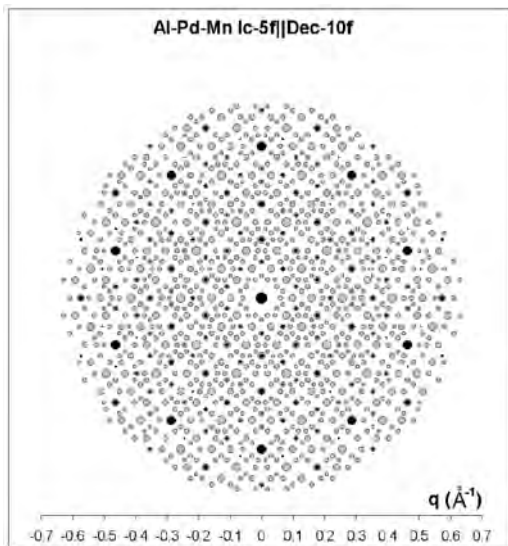


FIG. 5. Simulated configuration for Al-Pd-Mn icosahedral-decagonal epitaxy. Gray and black spots represent the decagonal and icosahedral spots, respectively.

quasiperiodic nature of the misfit strain field of the decagonal phase. Nevertheless, more work needs to be done to relate the strain due to κ and the observed dislocation density in crystal-quasicrystal epitaxy.

V. CONCLUSION

We have developed a coincidence reciprocal lattice plane model to calculate the interfacial energy for quasicrystal-crystal epitaxy based on Fletcher’s original work. This simple model is able to explain and predict most of the experimentally observed relative orientations for epitaxy as reported in literature. This model uses the coincidence of the reciprocal lattice planes to calculate the energy of the interface; a higher degree of coincidence results in lower energy interface.

Some difficulties to fit the simulated and observed configurations may arise from the kinetics of the system, resulting in a metastable configuration. Nevertheless, all experimental configurations appear as local minima in the energy-

calculations. The nature of the currently unknown interaction potential model requires further development; nonetheless, the combination of exponential form for the potential model and q -space cutoff appears to work very well for all tested cases. As the understanding of surface structures of quasicrystals improves, a better model for the surface reciprocal lattices can be constructed.

We show that with this simple approach epitaxial relation-

ships between crystals and quasicrystals can be established relatively accurately.

ACKNOWLEDGMENTS

Arun Subramanian provided valuable comments and suggestions. This work was supported by U.S. Air Force Office of Scientific Research—Department of Defense through Grant No. F49620-96-0214.

*Electronic address: e-widjaja@northwestern.edu

- ¹K. Urban, N. Moser, and H. Kronmüller, *Phys. Status Solidi A* **91**, 411 (1985).
- ²M. Zurkirch, B. Bolliger, M. Erbudak, and A.R. Kortan, *Phys. Rev. B* **58**, 14 113 (1998).
- ³Y.L. Qin, R.H. Wang, Q.L. Wang, Y.M. Zhang, and C.X. Pan, *Philos. Mag. Lett.* **71**, 83 (1995).
- ⁴X.X. Yang, R.H. Wang, and X.J. Fan, *Philos. Mag. Lett.* **73**, 121 (1996).
- ⁵Z. Shen, M.J. Kramer, C.J. Jenks, A.I. Goldman, T. Lograsso, D. Delaney, M. Heinzig, W. Raberg, and P.A. Thiel, *Phys. Rev. B* **58**, 9961 (1998).
- ⁶Z. Zhang and W. Geng, *Philos. Mag. Lett.* **65**, 211 (1992).
- ⁷Z. Zhang and K. Urban, *Scr. Metall. Mater.* **23**, 1663 (1989).
- ⁸Y. Zhuang, Z. Zhang, and D.B. Williams, *J. Non-Cryst. Solids* **153**, 119 (1993).
- ⁹M. Shimoda, T.J. Sato, A.P. Tsai, and J.Q. Guo, *Phys. Rev. B* **62**, 11 288 (2000).
- ¹⁰M. Shimoda, J.Q. Guo, T.J. Sato, and A.P. Tsai, *Surf. Sci.* **482**, 784 (2001).
- ¹¹M. Shimoda, T.J. Sato, A.P. Tsai, and J.Q. Guo, *Surf. Sci.* **507**, 276 (2002).
- ¹²E.J. Widjaja and L.D. Marks, *Philos. Mag. Lett.* **83**, 47 (2003).
- ¹³B. Bolliger, M. Erbudak, D.D. Vvedensky, M. Zurkirch, and A.R. Kortan, *Phys. Rev. Lett.* **80**, 5369 (1998).
- ¹⁴G. Friedel, *Leçon de Cristallographie* (Berger Levrault, Paris, 1926).
- ¹⁵S. Ranganathan, *Acta Crystallogr.* **21**, 197 (1966).
- ¹⁶H. Grimmer, *Acta Crystallogr., Sect. A: Cryst. Phys., Diffr., Theor. Gen. Crystallogr.* **A30**, 685 (1974).
- ¹⁷H. Grimmer, *Acta Crystallogr., Sect. A: Cryst. Phys., Diffr., Theor. Gen. Crystallogr.* **A30**, 680 (1974).
- ¹⁸H. Grimmer, W. Bollmann, and D.H. Warrington, *Acta Crystallogr., Sect. A: Cryst. Phys., Diffr., Theor. Gen. Crystallogr.* **A30**, 197 (1974).
- ¹⁹H. Grimmer, *Acta Crystallogr., Sect. A: Cryst. Phys., Diffr., Theor. Gen. Crystallogr.* **A32**, 783 (1976).
- ²⁰D.H. Warrington, O. Radulescu, and R. Luck, *Acta Crystallogr., Sect. A: Found. Crystallogr.* **A53**, 314 (1997).
- ²¹M.A. Fortes, *Acta Crystallogr., Sect. A: Found. Crystallogr.* **A39**, 351 (1983).
- ²²R.K. Mandal and S. Lele, *Mater. Sci. Eng., C* **294**, 813 (2000).
- ²³N.H. Fletcher, *J. Appl. Phys.* **35**, 234 (1964).
- ²⁴N.H. Fletcher and K.W. Lodge, *Epitaxial Growth, Part B* (Academic Press, New York, 1975), Chap. 7, pp. 529–557.
- ²⁵C. Giacovazzo, *Direct Phasing in Crystallography* (Oxford University Press, New York, 1998), pp. 2, 18–20.
- ²⁶N.H. Fletcher, *Philos. Mag. Lett.* **16**, 159 (1967).
- ²⁷E. Clementi and D.L. Raimondi, *J. Chem. Phys.* **38**, 2686 (1963).
- ²⁸E. Clementi, D.L. Raimondi, and W. Reinhard, *J. Chem. Phys.* **47**, 1300 (1967).
- ²⁹B. Bolliger, V.E. Dmitrienko, M. Erbudak, R. Luscher, H.U. Nissen, and A.R. Kortan, *Phys. Rev. B* **63**, 052203 (2001).
- ³⁰K.J. Franke, H.R. Sharma, W. Theis, P. Gille, P. Ebert, and K.H. Rieder, *Phys. Rev. Lett.* **89**, 156104 (2002).
- ³¹G.H. Li, D.L. Zhang, H.W. Jiang, W.Y. Lai, W. Liu, and Y.P. Wang, *Appl. Phys. Lett.* **71**, 897 (1997).
- ³²Bolliger *et al.* (Ref. 29) reported epitaxial textures of fcc Al on icosahedral Al-Pd-Mn quasicrystal. However, this paper does not report the interface relationship between the fcc Al and the fivefold surface of icosahedral Al-Pd-Mn; instead it reports the alignment of [111] axes of fcc Al with one of five threefold-symmetry axes of the substrate quasicrystal at 37.37° away from the surface normal. Franke *et al.* (Ref. 30) reported a quasicrystalline epitaxial single element (antimony and bismuth) monolayer on icosahedral Al-Pd-Mn and decagonal Al-Ni-Co quasicrystal surfaces. Li *et al.* (Ref. 31) reported growth of epitaxial Al-Cu-Co decagonal on alumina substrates using x-ray diffraction but was unable to study the geometric orientations at the interface.
- ³³Z.G. Wang, X.X. Yang, and R.H. Wang, *J. Phys.: Condens. Matter* **5**, 7569 (1993).
- ³⁴S. Weber, computer code QUAREF, 2000 (private communication).
- ³⁵M. Dai and R. Wang, *Acta Crystallogr., Sect. B: Struct. Sci.* **46**, 455 (1990).
- ³⁶W. Steurer and K.H. Kuo, *Acta Crystallogr., Sect. B: Struct. Sci.* **46**, 703 (1990).
- ³⁷W. Steurer, T. Haibach, B. Zhang, S. Kek, and R. Luck, *Acta Crystallogr., Sect. B: Struct. Sci.* **49**, 661 (1993).
- ³⁸A. Yamamoto and K. Hiraga, *Mater. Sci. Eng., C* **294**, 228 (2000).
- ³⁹S. Weber and A. Yamamoto, *Acta Crystallogr., Sect. A: Found. Crystallogr.* **54**, 997 (1998).
- ⁴⁰M.V. Jaric, *Phys. Rev. B* **34**, 4685 (1986).
- ⁴¹O.K. Andersen, O. Jepsen, and D. Glotzel, *Highlights of Condensed-Matter Theory* (North-Holland Physics Publishing, Amsterdam, 1985), pp. 116–117.
- ⁴²C. Khokkaz, R. Galler, H. Mehrer, P.C. Canfield, I.R. Fisher, and M. Feuerbacher, *Mater. Sci. Eng., C* **294**, 697 (2000).
- ⁴³P.J. Steinhardt, H.C. Jeong, K. Saitoh, M. Tanaka, E. Abe, and A.P. Tsai, *Nature (London)* **396**, 55 (1998).
- ⁴⁴T. Zunkley and H. Nakajima, *Philos. Mag. A* **80**, 1065 (2000).
- ⁴⁵Z. Shen *et al.*, *Surf. Sci.* **450**, 1 (2000).
- ⁴⁶T. Cai *et al.*, *Surf. Sci.* **495**, 19 (2001).
- ⁴⁷M. Shimoda, J.Q. Guo, T.J. Sato, and A.P. Tsai, *Surf. Sci.* **454**, 11 (2000).
- ⁴⁸D. Naumovic, P. Aebi, L. Schlapbach, C. Beeli, K. Kunze, T.A. Lograsso, and D.W. Delaney, *Phys. Rev. Lett.* **87**, 195506 (2001).

- ⁴⁹B. Bolliger, M. Erbudak, D.D. Vvedensky, and A.R. Kortan, Phys. Rev. Lett. **82**, 763 (1999).
- ⁵⁰While most reports confirmed a similar quasiperiodic surface phase as in the bulk (for example, Refs. 45–47 Naumovic *et al.* (Ref. 48), and Bolliger *et al.* (Ref. 49) reported a formation of a stable decagonal quasicrystalline Al-Pd-Mn surface layer on a Al-Pd-Mn icosahedral single crystal by sputtering and annealing.
- ⁵¹N. Menguy, M. Audier, M. DeBoissieu, P. Guyot, M. Boudard, and C. Janot, Philos. Mag. Lett. **67**, 35 (1993).
- ⁵²W. Sun and K. Hiraga, Philos. Mag. Lett. **67**, 159 (1993).
- ⁵³Z. Zhang and N.C. Li, Scr. Metall. Mater. **24**, 1329 (1990).